Journal of Nuclear Materials 390–391 (2009) 242–245

Contents lists available at ScienceDirect

Journal of Nuclear Materials

journal homepage: www.elsevier.com/locate/jnucmat

Sensitivity of injected argon behavior to changes in magnetic balance in double-null plasmas in DIII-D

T.W. Petrie [a,*], N.H. Brooks [a], M.E. Fenstermacher [b], M. Groth [b], A.W. Hyatt [a], C.J. Lasnier [b], A.W. Leonard [a], G.D. Porter [b], M.J. Schaffer [a], M.R. Wade [a], J.G. Watkins [c], W.P. West [a]

[a] General Atomics, P.O. Box 85608, San Diego, CA 92186-5608, USA
[b] Lawrence Livermore National Laboratory, P.O. Box 808, Livermore, CA 94551, USA
[c] Sandia National Laboratories, P.O. Box 5800, Albuquerque, NM 87185, USA

ARTICLE INFO

PACS:
52.55.Fa
52.25.V
52.55.Rk
28.52.Cx

ABSTRACT

Recent DIII-D experiments show that both magnetic balance and particle drifts are important to understanding how argon impurities accumulate in balanced and unbalanced double-null plasmas during 'puff and pump' radiating divertor operation. Unbalanced double-null shapes, which are biased in the direction opposite to the ion $\mathbf{B}\times\nabla\mathbf{B}$ drift direction, have produced the best result to-date in terms of coupling a radiating divertor approach with an H-mode plasma. The proximity to balanced double-null that can be used for puff-and-pump may depend on the width of the heat flux profile in the scrape-off layer. A comparison of plasma behavior in the open lower divertor to that of the more closed upper divertor determined that plasma density control was far more sensitive to the ion $\mathbf{B}\times\nabla\mathbf{B}$ drift direction than to the relative closure of the divertor.

1. Introduction

The conceptual designs for high powered, high-performance tokamaks are typically based on double-null plasma shaping for good confinement and stability, but plasma heating of the divertor targets presents a major problem. One proposed solution to this heating problem involves artificially enhancing the radiated power in the divertor and the plasma 'mantle' by 'seeding' the divertor with impurities. For this approach to be practical, however, the confinement and stability of the plasma core cannot be compromised by significant penetration of the seeded impurity into the main plasma. Such leakage can be reduced by increasing the flow of deuterium ions into the divertor with a combination of upstream deuterium gas-puffing and particle pumping at the divertor targets, i.e., 'puff-and-pump' [1–5].

Successful coupling of a puff-and-pump radiating divertor with ELMing H-mode conditions was demonstrated for a double-null shape that was biased in the direction *away* from the ion $\mathbf{B}\times\nabla\mathbf{B}$ drift direction with a magnetic imbalance parameter $dRsep = 1.2$ cm and argon as the seed impurity: $\tau_E/\tau_{89P} = 2$, $\beta_N = 2.4$, $n_e/n_{eG} = 0.6$, $P_{RAD}/P_{inj} \approx 0.6$, and a peak heat flux reduction at the outer divertor target of ≈ 2.5 [4]. (*dRsep* is defined as the radial distance between the upper divertor separatrix and the lower divertor separatrix at the outer midplane.) This result was in contrast to an earlier puff-and-pump study on DIII-D, where a marked accumulation of argon in the core plasma resulted in poor performance [1]. The direction of the ion $\mathbf{B}\times\nabla\mathbf{B}$ drift had been shown to have a dramatic effect on both plasma recycling [6] and particle pumping [7]. This led to the suspicion that the ion $\mathbf{B}\times\nabla\mathbf{B}$ drift direction might also be affecting puff-and-pump behavior, since the direction of the ion $\mathbf{B}\times\nabla\mathbf{B}$ drift in Ref. [4] was out of the divertor and oppositely directed in Ref. [1]. Variation in *dRsep* had also been shown to have a strong effect on plasma behavior [6,7].

In this paper we focus on how changing the direction the ion $\mathbf{B}\times\nabla\mathbf{B}$ drift and the divertor magnetic balance can affect puff-and-pump performance, particularly in how injected impurities accumulate in the core plasma.

2. Experimental description

We exploit the capabilities of DIII-D to make both balanced double-null (BDN) and unbalanced double-null (UDN) shapes in high-triangularity, and then to pump these shapes from both divertors simultaneously (Fig. 1). In addition to deuterium, the three cryopumps also remove argon atoms, the seed impurity for these experiments. Argon was selected because it radiates effectively at the temperatures prevailing in the divertor and pedestal regions of DIII-D H-mode plasmas and has a relatively short ionization mean-free path.

To increase the D^+ ion flow into toward these pumps, deuterium gas (D_2) was introduced upstream from the low-field side of the

* Corresponding author.
E-mail address: petrie@fusion.gat.com (T.W. Petrie).

0022-3115/$ - see front matter © 2009 Elsevier B.V. All rights reserved.
doi:10.1016/j.jnucmat.2009.01.071

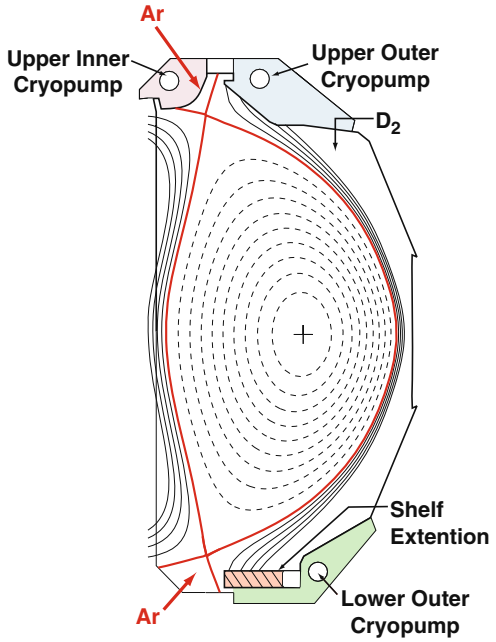

Fig. 1. The particle pumping- and gas injection locations are superimposed on the poloidal plasma cross-section of a balanced DN plasma. Argon can be injected into the private flux region of either divertor.

core plasma, as shown in Fig. 1. Argon was injected into the private flux region (PFR) of upper divertor. The parameters for the ELMing H-mode plasmas discussed in this study were: $\bar{n}_e \approx (0.5\text{–}0.8)\times 10^{20}$ m^{-3} (or $\bar{n}_e/n_G \approx 0.4\text{–}0.7$, where n_G is the Greenwald density), and $H_{89P} = 1.5\text{–}2.0$ [or $H_{98}(y,2) = 0.9\text{–}1.2$]. In this study *dRsep* ranges from −1.5 cm to +1.5 cm. We refer to configurations with $|dRsep| \geqslant 1$ cm as 'single null' (SN) even though the secondary null remains within the vacuum vessel.

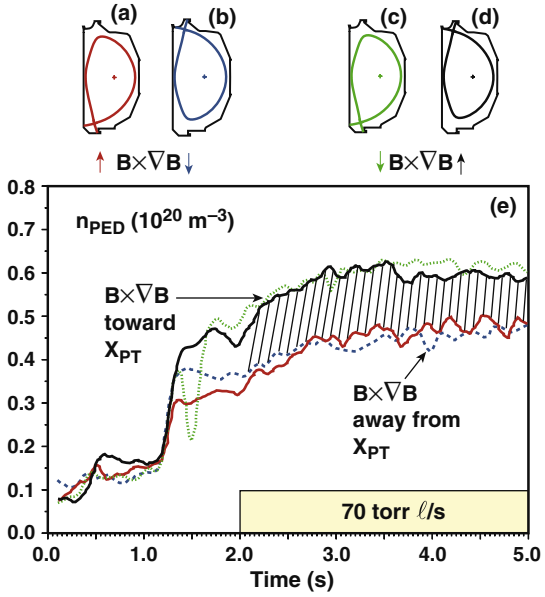

Fig. 2. (a–d) The four plasma arrangements discussed in Section 3.1 are shown, together with the direction of the ion $\mathbf{B}\times\nabla\mathbf{B}$ drift direction relative to their divertor. (e) The pedestal density is correlated more with the ion $\mathbf{B}\times\nabla\mathbf{B}$ drift direction than with differences in divertor structure.

3. Results

3.1. Effect of the $\mathbf{B}\times\nabla\mathbf{B}$ direction on plasma fueling

In these experiments, changes in the pedestal density n_{PED} correlated more strongly with the ion $\mathbf{B}\times\nabla\mathbf{B}$ drift direction than with differences in the upper and lower divertor geometry. As can be seen in Fig. 1, the upper divertor structure in DIII-D is more closed than the lower. Fig. 2(a–d) shows four distinct SN arrangements, differentiated by the ion $\mathbf{B}\times\nabla\mathbf{B}$ drift direction and the location of the primary divertor relative to the upper or lower divertor structures. The direction of the ion $\mathbf{B}\times\nabla\mathbf{B}$ drift was *away from* the divertor in Fig. 2(a and b) and *toward* the divertor in Fig. 2(c and d). There were two basic configurations, classified as either lower divertor (Fig. 2(a and c)) or upper divertor (Fig. 2(b and d)). In each case, the deuterium gas puff rate Γ_{D_2} was 70 torr l/s (0.47×10^{22} particles/s). To match particle exhaust characteristics in the four cases, only the lower outer pump was activated for the cases in Fig. 2(a and c) and only the upper outer pump was activated for the cases in Fig. 2(b and d). The pedestal density for the two cases with the ion $\mathbf{B}\times\nabla\mathbf{B}$ drift direction *toward* the dominant divertor was ≈30% greater than for the two cases *away from* the dominant divertor (Fig. 2(e)). Thus, the different closures of the upper and lower divertor had little effect on n_{PED}.

3.2. Effect of changing the ion $\mathbf{B}\times\nabla\mathbf{B}$ direction on argon behavior in SN plasmas

Both the accumulation of argon inside the core plasma and the removal of argon from the dominant divertor were both sensitive to the ion $\mathbf{B}\times\nabla\mathbf{B}$ drift direction. This is shown for two upper SN plasmas similar to Fig. 2(b), but with opposite ion $\mathbf{B}\times\nabla\mathbf{B}$ drift direction. Both have the same Γ_{D_2} (=108 torr l/s or 0.72×10^{22} particles/s) and argon puff rate Γ_{AR} (=1 torr l/s or 3.3×10^{19} particles/s), (Fig. 3(a)). Consistent with Fig. 2, the pedestal density was higher for the case with the ion $\mathbf{B}\times\nabla\mathbf{B}$ drift direction toward the divertor (Fig. 3(b)). The inner leg of the divertor partially-detached near $t = 3.6$ s, where the divertor radiated power $P_{R,DIV}$ shows a pronounced increase (Fig. 3(c)). Argon accumulation in the core was ≈3.5 times higher for the ion $\mathbf{B}\times\nabla\mathbf{B}$ drift direction toward the dominant divertor, as evidenced by the density of the dominant Ar^{16+} charge state $n_{Ar^{+16}}$ at $\rho = 0.7$, which was located ≈10 cm inboard of the outer midplane separatrix (Fig. 3(d)); for similar discharges, detailed analysis with the MIST [8] impurity transport code indicates that $n_{Ar^{+16}}$ should be >80% of n_{Ar} at $\rho = 0.7$. The carbon density n_C in the core increased slightly during argon injection, as evidenced by the density of the dominant C^{6+} charge state at $\rho = 0.7$ (Fig. 3(e)). However, the carbon contribution to $Z_{eff}(\rho = 0.7)$ did not increase during argon injection for either case because n_e had also increased. The rise in Z_{eff} that results from argon injection is almost entirely due to argon accumulation in the core plasma, i.e., 1.45–1.67 for $\mathbf{B}\times\nabla\mathbf{B}$ toward the dominant divertor and 1.67–1.73 for $\mathbf{B}\times\nabla\mathbf{B}$ for $\mathbf{B}\times\nabla\mathbf{B}$ away from the divertor. For this case, the argon pumping rate of the outer divertor leg $\Gamma_{P\text{-}AR}$ was much higher than with the ion $\mathbf{B}\times\nabla\mathbf{B}$ drift direction toward the dominant divertor (Fig. 3(f)), i.e., ≈85% of the argon was removed by the upper outer divertor pump when the ion $\mathbf{B}\times\nabla\mathbf{B}$ drift direction was away from the X-point versus ≈35% removed by this same pump.

3.3. Comparison of SN with DN plasmas during puff-and-pump operation

Recent experiments have shown that argon densities in the core plasma are comparable for DN ($dRsep = 0$) and SN ($dRsep =$

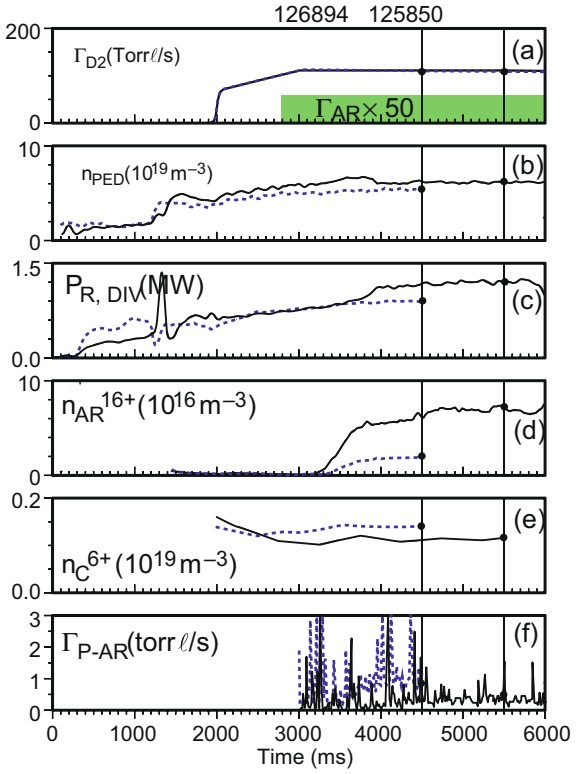

Fig. 3. (a) The waveforms of the Γ_{D_2} and Γ_{AR} gas puff programs, (b) n_{PED}, (c) $P_{R.DIV}$, $n_{AR^{16+}}$ at $\rho = 0.7$, (e) n_C at $\rho = 0.7$ and (f) $\Gamma_{P\text{-}AR}$ are shown as a function of time. The ion $\mathbf{B} \times \nabla\mathbf{B}$ drift direction is toward the divertor (solid) and away from the divertor (dashed).

+1.2 cm) at lower values of Γ_{D_2} but differ significantly at the highest Γ_{D_2} (Fig. 4). For both DN and SN cases, the ion $\mathbf{B} \times \nabla\mathbf{B}$ drift was directed away from the dominant divertor of the SN into which the argon was injected. For both DN and SN cases for $\Gamma_{D_2} \leqslant 70$ torr l/s, the argon concentrations were comparable for a given Γ_{D_2} and were reduced when Γ_{D_2} was increased. However, when Γ_{D_2} was raised to ≈100 torr l/s, the argon concentration for the BDN increased sharply, while the argon concentration continued to decrease in the SN case. The inner divertor leg of the DN at the highest Γ_{D_2} was tenuously attached (e.g., electron density (n_{IN-DIV}) and temperature T_{IN-DIV} were typically $\leqslant 1 \times 10^{19}$ m^{-3} and ⩽10 eV, respectively, at the inner divertor target) during the deuterium and argon gas-puffing phase. This may have provided an escape route for the argon out of the divertor. For the SN case

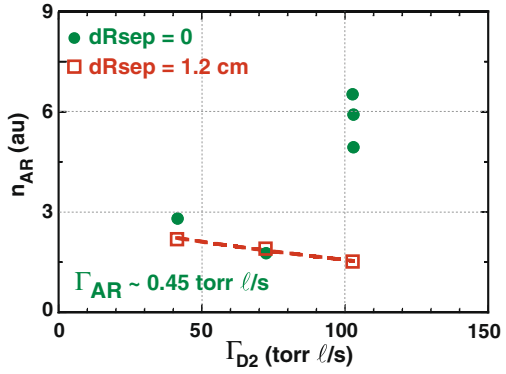

Fig. 4. Argon densities in the main plasma are shown as a function of the deuterium gas puff rate Γ_{D_2} for both DN and SN.

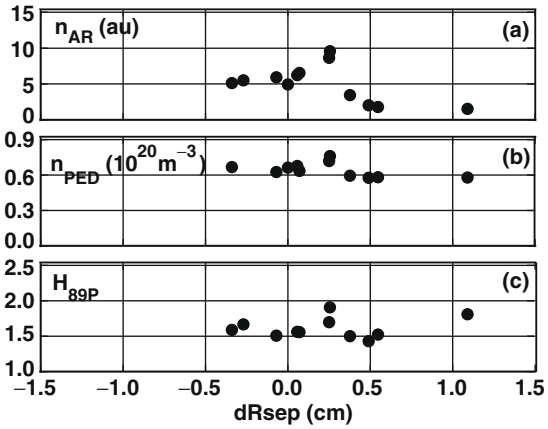

Fig. 5. (a) n_{AR}, (b) n_{PED}, and (c) H_{89P} are shown as a function of *dRsep*.

where n_{IN-DIV} and T_{IN-DIV} were ≈ 10^{20} m^{-3} and 10–20 eV, respectively, argon escape through the inner leg would be less likely, since the mean-free path of neutral argon would be at least an order of magnitude smaller than for the SN case.

3.4. Argon accumulation into the core plasma near-DN

The data indicate that the argon buildup in the core plasma of the SN is significantly lower than that of the DN, if the ion $\mathbf{B} \times \nabla\mathbf{B}$ drift is directed is away from the dominant divertor and *dRsep* ⩾ 0.4 cm. Fig. 5(a) shows argon concentration in the plasma core (a), the ITER normalized confinement time (b), and the pedestal density (c), as a function of *dRsep*. The argon concentration decreased by about a factor of three between *dRsep* = 0 and *dRsep* = +0.4 cm. A peak in both n_{AR} and n_{PED} near +0.25 cm, was likely associated with an improvement in energy confinement. Since $H_{89P} \approx 1.5$ [$H_{98}(y,2) = 0.9$] for both *dRsep* = 0 and *dRsep* = 0.4 cm cases, however, the observed change in n_{AR} was not due to the change in confinement time.

4. Discussion

Pedestal density was much more dependent on the direction of the ion $\mathbf{B} \times \nabla\mathbf{B}$ drift than on differences of the DIII-D divertor closure. The importance of particle drifts in fueling has previously been discussed in Ref. [9], where the authors also showed that the most significant fueling of the core plasma occurred on the high-field side of the X-point. As such, the differences between upper and lower divertors would have a secondary role in fueling.

The direction of the net particle flow across the PFR plays an important role in determining whether the argon that is injected into the PFR is pushed toward the inner or outer divertor target. UEDGE [10] edge transport analysis was applied to the two cases discussed in Section 3.2. Using a geometry which spans both the primary and secondary separatrices, UEDGE modeling of the particle flows in and near the divertor region indicates that the net deuterium particle flow across the PFR (1) is directed across the PFR toward the inboard divertor target for the ion $\mathbf{B} \times \nabla\mathbf{B}$ into the divertor and (2) is reversed when the ion $\mathbf{B} \times \nabla\mathbf{B}$ drift is reversed. UEDGE predicts that the $E_r \times B$ drift is largely responsible for determining the direction of these particle flows in the PFR, where E_r is the radial electric field determined largely by the electron temperature gradient normal to the local flux surfaces. Previously these poloidal particle flows were measured in DIII-D and found to be consistent with the particle flow predicted by modeling [11].

From UEDGE analysis, the argon in the PFR is preferentially swept by the $E_r \times B$ drift toward the inner target for the case with

the ion $\mathbf{B} \times \nabla \mathbf{B}$ toward the divertor, and then toward the lower divertor on the high-field side SOL, again largely driven by the $E_r \times B$ drift. The increase in argon at the inner target enhances the local radiated power, which can result in a partially-detached inner divertor leg, as occurred for the case with the ion $\mathbf{B} \times \nabla \mathbf{B}$ toward the divertor in Fig. 3. The argon then has a more direct route to the core via the relatively cool plasma on the high-field side (HFS) of the X-point. For $\mathbf{B} \times \nabla \mathbf{B}$ away from the dominant divertor, however, the injected argon was preferentially swept toward the outer divertor target, where it could also recycle and radiate. Electron temperature (and the peak heat flux) was reduced, but detachment of the outboard leg from the divertor target was not observed for the levels of argon and deuterium injection rates used in this experiment. That more argon was swept toward the outer target was reflected by the fact that significantly more argon was exhausted by the upper outer divertor cryopump (Fig. 3(f)).

Low $n_{\mathrm{IN-DIV}}$ and $T_{\mathrm{IN-DIV}}$ at the inner target of the DN cases discussed in Section 3.3 facilitated the escape of argon from the divertor. These conditions were typical in DN plasmas, in contrast to the SN ($dRsep = +1.2$ cm) plasmas with similar gas-puffing and power input. We note that the power flow out of the core plasma is primarily on its low-field side (LFS) [12]. Since the LFS is magnetically connected to the HFS for the SN, roughly half of the power entering the SOL on the LFS is (in principle) available to maintain plasma attachment at the inner divertor target [13]. For a DN, however, the LFS is magnetically isolated from the HFS; power flow entering the SOL on the LFS is shunted into the two outer divertor targets, and is unavailable to maintain plasma ionization at the inner divertor targets. While the power flowing out of the plasma on the high-field side of the DN was sufficient in supplying enough power to keep the inner targets attached at low Γ_{D_2} (Fig. 4), the increase in both core and divertor radiated power for the case with $\Gamma_{D_2} = 100$ torr l/s made it more difficult to maintain sufficiently attached divertor conditions at the inner targets.

However, as the magnetic balance shifts from DN to SN, a larger fraction of power that flows into the LFS of the SOL transits to the inner target. In Section 3.4, we found that significant buildup of argon in the core plasma resembled that of the 'single-null' case only after *dRsep* had reached approximately +0.4–0.5 cm. Previous heat flux measurements for very similar discharges as discussed here indicate that the width of the heat flux profile λ_P was also 0.4–0.5 cm [12]. Hence, much of the power flow into the LFS of the SOL would no longer be shunted into the lower divertor but instead now follow the SOL field lines around to the inner divertor target. Thus, for $dRsep \approx \lambda_P$, conditions would be more favorable for maintaining the density and temperature needed to impede the escape of argon to the HFS. Increasing *dRsep* would lead to further would lead to still more power reaching the inner target, but this increase would be modest. Hence, in terms of the plasma that the argon 'sees' at the inner target, discharges with $dRsep \geqslant 0.4$ cm resemble the 'single-null' ($dRsep = 1.1$ cm) plasmas much more than the BDN plasmas. We are presently working with the UEDGE code to address this issue quantitatively.

5. Conclusion

In designing future generation high-performance tokamaks, which are very likely to be based on DN or near-DN plasma shapes, we must carefully assess the contributions of both particle drifts and magnetic balance, particularly if the puff-and-pump radiating divertor approach is under consideration. For tokamaks characterized as largely single-null, such as ITER, the results presented here point to the importance of considering particle drifts in assessing the projected success (1) of achieving and maintaining a detached inner divertor leg using seed impurities as a 'trigger', (2) of preventing the seed impurity from contaminating the main plasma, and (3) even of operating as an unbalanced DN, as might occur in more triangular, high-performance ITER plasmas.

Acknowledgments

This work was supported by the US Department of Energy under DE-FC02-04ER54698, DE-AC52-07NA27344, and DE-AC04-94AL85000.

References

[1] M.R. Wade et al., Nucl. Fusion 38 (1998) 1839.
[2] J. Rapp et al., Nucl. Fusion 44 (2004) 312.
[3] A. Kallenbach et al., J. Nucl. Mater. 337–339 (2005) 732.
[4] T.W. Petrie et al., J. Nucl. Mater. 363–365 (2007) 416.
[5] T.W. Petrie et al., Nucl. Fusion 48 (2008) 045010.
[6] T.W. Petrie et al., J. Nucl. Mater. 313–316 (2003) 834.
[7] T.W. Petrie et al., Nucl. Fusion 46 (2006) 57.
[8] R.A. Hulse, Nucl. Technol. Fusion 3 (1983) 259.
[9] M. Groth et al., J. Nucl. Mater. 337–339 (2005) 425.
[10] T.D. Rognlien et al., Phys. Plasmas 34 (1994) 362.
[11] J.A. Boedo et al., Phys. Plasmas 7 (2000) 1075.
[12] T.W. Petrie et al., J. Nucl. Mater. 290–293 (2001) 935.
[13] A.W. Leonard et al., J. Nucl. Mater. 220–222 (1995) 325.